

Impact Evaluation Approach of a Texture Cross Section Shape on Hydrodynamic Lubrication Performance

Xia He, Wenling Liao, Guorong Wang and Mengyuan Li

Abstract It has been confirmed that bionic surface texture can effectively improve the lubricating and tribological performance of the sliding surface, and the texture cross section shape and depth are important parameters affecting the lubrication performance of the texture. However, there is a lack of effective optimization method for a texture cross section shape and determining the texture depth of a random texture cross section shape. Hydrodynamic lubrication performance model of a single texture under the incompressible Newtonian fluid lubrication conditions was established based on the two dimensional steady-state Reynolds equation and texture depth equation, and finite difference method was adopted to discrete and solve the distribution of oil film pressure on the textured surface as well as analyzes the impact of different texture cross section shapes and depth on oil film pressure distribution and surface load capacity. The numerical simulation result shows that the textured surface can obtain a better hydrodynamic lubrication performance by guaranteeing that the average texture depth of a random shape of texture cross section equals the initial thickness of oil film. In addition, the shape of a texture cross section can be optimized based on the method of smaller a texture depth and deviation of a texture depth so as to obtain the optimal hydrodynamic lubrication performance of textured surface.

Keywords Surface texture · Texture depth · Texture cross section shape
Hydrodynamic lubrication performance · Optimization method

X. He · W. Liao (✉) · G. Wang · M. Li
School of Mechatronic Engineering, Southwest Petroleum University,
Chengdu 610500, China
e-mail: lwswpi16@163.com

X. He
e-mail: hexia@swpu.edu.cn

1 Introduction

During the process of designing mechanical products, reliability, performance and service life are the major factors that should be considered. Improving the performance and service life of mechanical products has an important effect on increasing their market competitiveness whereas the friction and wear on the matching surface of various mechanical parts are also a significant factor affecting the performance and service life of the mechanical system. In recent years, researchers have made exploration and analysis [1–3] from various aspects on how to enhance the lubrication performance on the surface of friction pair and reduce the friction and wear. Considering the phenomenon that the epidermis of creatures in the nature has a special structure but with a sound effect on reducing friction, the bionic surface texture technology was put forward to be used in lubrication and friction reduction of the mechanical system. Based on the experimental and theoretical methods for solving the Reynolds equation [4–6] and CFD [7–9], the impact and its laws of bionic surface texture on lubrication as well as friction and wear was studied. The result indicates that, based on the influence mechanism under different lubrication conditions: (1) Under the condition of dry friction, the bionic surface texture can effectively capture abrasion dust and reduce the secondary wear caused by abrasion dust [10]; (2) Under the condition of mixed lubrication or boundary lubrication, the texture can store and provide lubrication medium for the surface of friction pair, thus keeping such surfaces stay at the lubrication state for a long time [11]; (3) Under the lubrication state of full oil film, the micro fluid hydrodynamic pressure produced by the texture can effectively enhance the load capacity of the surface [12], bionic surface texture can effective increase the lubrication performance on the friction pair surface and reduce friction and wear. At present, the research outcomes from theories and experiments have promoted the application of the bionic surface texture to the fields of piston-cylinder liner [13], sliding bearing [14] and computer disc [15], etc.

However, although the lubrication and friction reduction effect of the bionic surface texture has been confirmed by theoretical and experimental methods, and the surface texture technologies have been well applied to some fields, not all parameter for textures can play a positive role [16–18]. The type of texture, area ratio and depth of texture and the texture cross section shape etc. are important parameters affecting the lubrication and friction reduction performance of the texture [19–25]. Therefore, optimization of texture parameters is still a focus in the study of texture. The differences in the impact of different texture cross section shapes on the hydrodynamic lubrication performance have been analyzed based on virtual texture and numerical simulation methods by Nanbu et al. [26]. The result shows that compared with flat cross section texture, micro-wedge type and micro-step type textures at the bottom can effectively improve the pressure of lubrication oil film. Cui et al. [27] adopted grid method to carry out numerical study on the impact of different cross section micro grooves on the micro-channel flow drag reduction and pressure loss performance. The result indicates that different

shapes of cross section have different effect on friction reduction with the drag reduction coefficient of ridge-shape groove larger than V-shape groove, followed by shield-squamous shape groove and rib groove. Based on the geometry model of reciprocating sliding plane, geometry model of texture and Reynolds equation of fluid hydrodynamic pressure, Ji et al. [28] established theoretical models on the bearing of micro-groove textures of different cross section (parabolic cross section, triangular cross section and rectangular cross section), and analyzed the impact of texture on lubricating performance of the bearing. The result shows that angular variation of groove texture of rectangular cross section has the greatest impact on the average pressure of oil film while the triangular cross section has the least impact. Shen and Khonsari [29] adopted Anton Paar's multi-functional torsion rheometer to carry out the lubricating performance experiment on laser processing internal structures of rectangles, oblique triangle and dimple texture of isosceles triangle textures under a full oil film lubrication state. The result shows that the rectangular shape of cross section among three kinds of cross section textures has the largest load capacity on the surface. In addition, according to a research on the impact of texture depth on lubricating performance, Ronen et al. [30] studied the impact of texture on the lubricating performance of piston/cylinder system based on the Reynolds and motion equation, and topped out the dimple texture with the depth-diameter ratio of 0.1–0.18. Qiu et al. [24] studied the impact of texture cross section shape on the load capacity of parallel sliding bearing of lubricated gas. The analysis result shows that the optimal texture depth-diameter ratio parameter range is between 0.001 and 0.01, but the texture depth-diameter ratio has a smaller impact on the load capacity of sliding bearing compared to the rest of texture parameters. Based on N–S equation, Han et al. [31] established a three-dimensional hydrodynamic lubrication performance model of a single spherical micro-pit texture under incompressible Newtonian fluid lubrication and studied the relationship between three-dimensional pressure field of surface lubricating oil film, velocity field and texture. He pointed out that the optimal texture depth rendered the largest surface load capacity and topped out the no-dimensional dimple at the depth variation range of 0.8–2. Papadopoulos et al. [32] adopted computational fluid dynamics (CFD) software to analyze the impact of texture and its parameters on thrust-bearing. The result indicated that the load capacity on the textured surface of bearing was the largest when the depth of dimple approached the thickness of the smallest oil film.

Although the above researches have pointed out that different shapes of cross section have different impact on the hydrodynamic lubrication performance on the textured surface, the mechanism of the impact on the shape of texture cross section have not been analyzed and discussed. Besides, researches about the impact of texture depth on lubrication performance showed that the optimal texture depth has a certain relationship with the thickness of the smallest oil film. There is no relative research on analyzing the impact and its mechanism of the shape of texture cross section and texture depth on the lubricating performance by combining the average depth of texture and the smallest thickness of lubricating oil film. Therefore, the paper establishes a theoretical model of single texture hydrodynamic lubrication

performance, based on Reynolds equation and different cross section texture depth equation, adopts a finite difference method to discrete equation and solves the pressure distribution of oil film on the textured surface, then figures out the surface load capacity. Based on the relationship between the average depth of different cross section texture and the smallest thickness of lubricating oil film, the paper analyzes the impact and its mechanism of the shape of texture cross section on the surface load capacity under the same conditions and puts forward the optimization method for the shape of different texture cross section and determining the better texture depth among random shapes of cross section textures under the thickness of the smallest lubricating oil film is ensured.

2 Models

2.1 Physical Model

In general, the size of friction pair is at meter or centimeter level whereas the micro-pit texture with the friction increased on its surface is at micrometer level. Hence, during the process of numerical analysis, friction pair can be roughly simplified as the relative sliding plane of finite length and width with cyclical distribution of texture. As is shown by Fig. 1, it is a cross section schematic diagram of a texture friction pair. The top surface sliding speed on the surface is U while the lower textured surface remains relatively static. The initial spacing between the two planes of friction pair is H_0 and the maximum depth of texture is H_p . Micro-pit texture is cyclically distributed in the direction of X . As oil film pressure on the cyclical distribution of texture surface also takes on a cyclical change, this paper only selects a single texture unit (Fig. 2) as a research object with the length as L , width as W and diameter as D . The value of each parameter is listed in Table 1.

2.2 Mathematical Model

In this thesis, the lubricant between friction pairs is assumed to be the incompressible Newtonian fluid and the viscosity and density of lubricant is constant.

Fig. 1 Schematic diagram of texture cross section

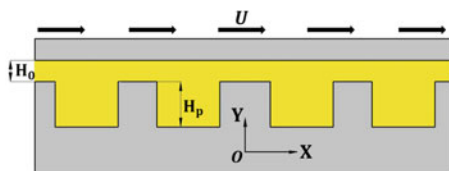


Fig. 2 Schematic diagram of texture unit

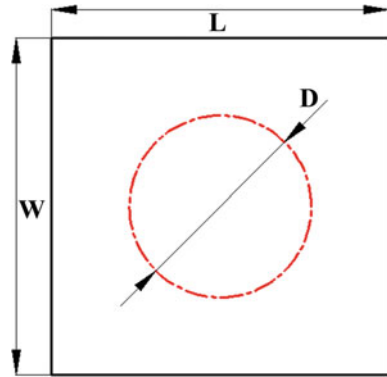


Table 1 Parameter of texture unit

Parameters	U (m/s)	H ₀ (μm)	H _p (μm)	L (μm)	W (μm)	D (μm)
Value	0.8	1/2	0.5; 1; 2; 4; 6; 8; 10	500	500	154.5

Moreover, the simulation analysis doesn't take the influence of temperature changing into consideration and the flow condition of lubricant is steady and laminar. Therefore, the two dimensional steady-state Reynolds equation of solving the film pressure distribution on the textured surface can be written as:

$$\frac{\partial}{\partial x} \left(h^3 \frac{\partial p}{\partial x} \right) + \frac{\partial}{\partial y} \left(h^3 \frac{\partial p}{\partial y} \right) = 6 u \eta \frac{\partial h}{\partial x} \tag{1}$$

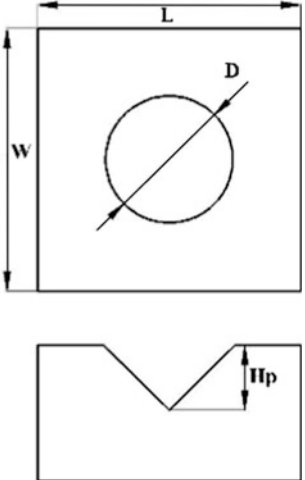
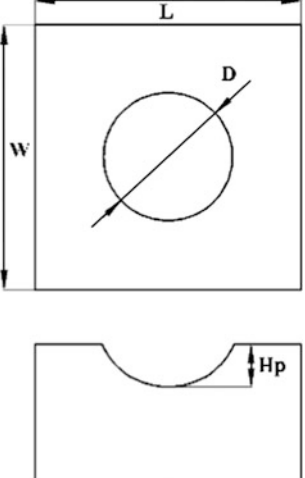
where x and y are the coordinates along and across the sliding direction, respectively; P is the local hydrodynamic pressure, h is the film thickness, u is the velocity; η the viscosity of the lubricant.

The film thickness h between friction pairs is related to the initial film thickness H₀ and the texture depth H_p. the depth of each point in the dimple texture of different cross sections is different. Expressions of film depth of six different cross sections are listed in Table 2. Combining with the parameters in Table 1, we can figure out the film depth of each point on the textured surface.

2.3 Simulating Calculation

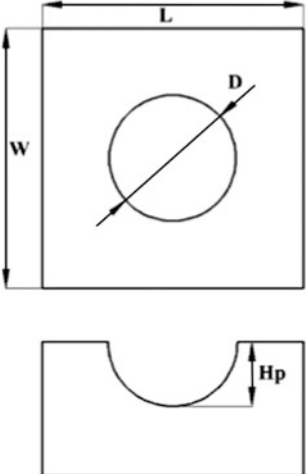
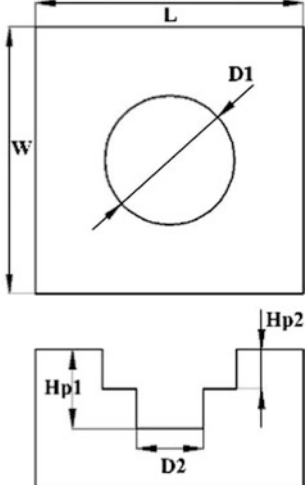
In the length (L) direction of texture unit, textures are distributed periodically. Thus, the periodically-distributed boundary condition of film pressure is used in the length direction of texture unit. In addition, in the width (W) direction of texture unit, the

Table 2 Parameters of film thickness of different cross section texture

Cross section shapes		Film depth
Triangle		$h = \begin{cases} H_0 & (x, y) \notin \Omega \\ H_0 + H_p - H_p * r & (x, y) \in \Omega \end{cases}$ $r = (x^2 + y^2)^{0.5} \quad \Omega : x^2 + y^2 < D^2/4$
Parabolic		$h = \begin{cases} H_0 & (x, y) \notin \Omega \\ H_0 + H_p * \cos(r * \pi/D) & (x, y) \in \Omega \end{cases}$ $r = (x^2 + y^2)^{0.5} \quad \Omega : x^2 + y^2 < D^2/4$

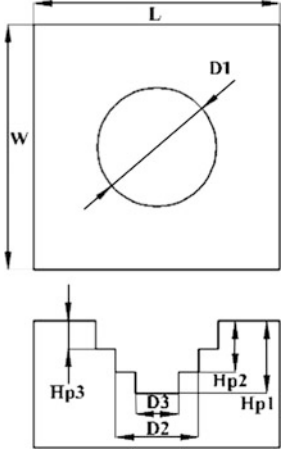
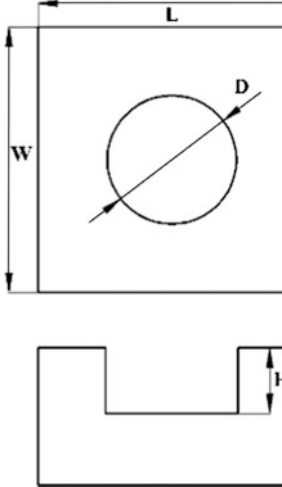
(continued)

Table 2 (continued)

Cross section shapes		Film depth
Circular arc		$h \begin{cases} H_0 & (x, y) \notin \Omega \\ H_0 + H_p * r & (x, y) \in \Omega \end{cases}$ $r = (1 - (2x/D)^2 - (2y/D)^2)^{0.5}$ $\Omega : x^2 + y^2 < D^2/4$
Second order type ladder		$h = \begin{cases} H_0 & (x, y) \in \Omega_0 \\ H_0 + H_{p1} & (x, y) \in \Omega_1 \\ H_0 + H_{p2} & (x, y) \in \Omega_2 \end{cases}$ $\Omega_0 : x^2 + y^2 \geq D_1^2/4 \quad \Omega_1 : x^2 + y^2 < D_2^2/4$ $\Omega_2 : x^2 + y^2 \geq D_2^2/4 \text{ and } x^2 + y^2 < D_1^2/4$

(continued)

Table 2 (continued)

Cross section shapes		Film depth
Three order type ladder		$h = \begin{cases} H_0 & (x, y) \in \Omega_0 \\ H_0 + H_{p1} & (x, y) \in \Omega_1 \\ H_0 + H_{p2} & (x, y) \in \Omega_2 \\ H_0 + H_{p3} & (x, y) \in \Omega_3 \end{cases}$ $\Omega_0 : x^2 + y^2 \geq D_1^2/4 \quad \Omega_1 : x^2 + y^2 < D_3^2/4$ $\Omega_2 : x^2 + y^2 \geq D_3^2/4 \text{ and } x^2 + y^2 < D_2^2/4$ $\Omega_3 : x^2 + y^2 \geq D_2^2/4 \text{ and } x^2 + y^2 < D_1^2/4$
Rectangle		$h = \begin{cases} H_0 & (x, y) \notin \Omega \\ H_0 + H_p & (x, y) \in \Omega \end{cases}$ $\Omega : x^2 + y^2 < D^2/4$

boundary film pressure in limited texture units is equal to the barometric pressure. Accordingly, in the process of simulating analysis, the boundary condition of film pressure, which is equal to barometric pressure, is used in the width direction of texture unit. Therefore, the boundary condition of film pressure can be expressed as:

$$p(x, y = 0) = p(x, y = W) = p_a \tag{2}$$

$$\frac{\partial p}{\partial x}(x = 0, y) = \frac{\partial p}{\partial x}(x = L, y) \tag{3}$$

$$p(x = 0, y) = p(x = L, y) \tag{4}$$

In the light of the time and accuracy of simulating calculation, the texture unit in this thesis is consists of 256×256 grid nodes. On the basis of boundary Eqs. (2), (3) and (4), we adopt the finite difference method and Gauss-Seidel iteration to solve the Reynolds equitation (1). Without regard to the influence of texture cavitation effect, the film pressure distribution on the texture unit has been got and the iteration convergence criterion of film pressure is:

$$\frac{\|P_{ij}^{k+1} - P_{ij}^k\|}{\|P_{ij}^k\|} \leq 10^{-5} \tag{5}$$

where $P_{i, j}$ is the pressure value at the point (i, j) , and K is the iterative time.

3 Results and Discussion

Figure 3 shows the changing curves that the load capacity of different cross section textured surface varies with the change of maximum texture depth when the initial film depth H_0 is 1 and 2 μm . In Fig. 3a, we can find that when the initial film depth is 1 μm and the maximum texture depth H_p is 0.5–10 μm , with the increasing of maximum texture depth, the load capacity of different shaped cross-section texture increases at first and then descends. However, because the shapes of cross sections are different, the scope of increasing and descending of load capacity within 0.5–10 μm maximum texture depth and the maximum texture depth corresponding to the maximum load capacity are also different. Meanwhile, the load capacity of rectangular cross section textured surface is very different from that of other cross section textured surface. That is, within the scope that the load capacity increases

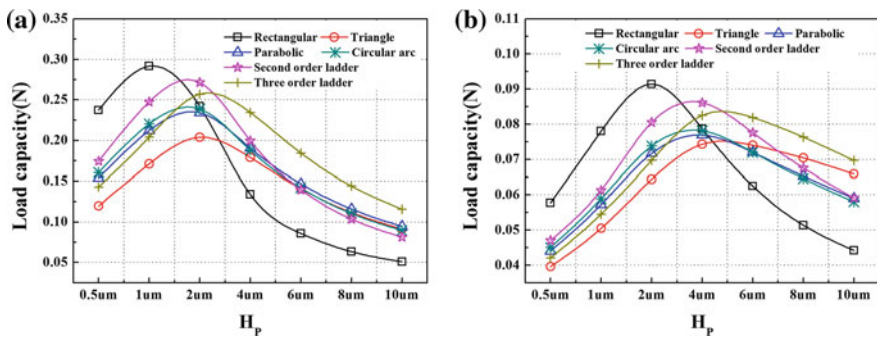


Fig. 3 The change law between maximum texture depth and load capacity: **a** $H_0 = 1 \mu\text{m}$; **b** $H_0 = 2 \mu\text{m}$

with the increasing of maximum texture depth, the load capacity of rectangular cross section textured surface is greater than that of other cross section textured surface; within the scope that the load capacity descends with the increasing of maximum texture depth, the load capacity of rectangular cross section textured surface descends faster than that of other cross section textured surface. When the maximum texture depth is in the scope of 4–10 μm , the load capacity of rectangular cross section textured surface will be less than that of other cross sections texture. Being similar to the change tendency in Fig. 3a, and b shows the same change law when the initial film thickness H_0 is 2 μm . But compared with the condition that the initial film thickness H_0 is 1 μm , when the texture depth is given, the maximum texture depth corresponding to the largest load capacity of different shaped cross-section texture is larger, which is similar to the study result of Papadopoulos et al. [32]. Namely, as the dimple depth gets closer to the minimum film thickness, the load capacity will become greater and the optimum texture depth will be increased with the increasing of initial film thickness.

Moreover, according to the different impact that different cross sections exerting on the load capacity with the same initial film thickness H_0 and texture depth H_P showed in Fig. 3, Table 3 provides the relation between maximum texture depth and average texture depth. According to Table 3, if the maximum texture depth H_P remains the same, the average texture depth of rectangular cross section texture ranks top, followed by second order ladder cross section texture, circular arc cross section texture, parabolic cross section texture, three order ladder and triangle cross section texture. Figure 4 describes the comparison between average texture depth and the load capacity when the maximum texture depth H_P is 1 and 2 μm . From Fig. 4a, we can find that if the maximum texture depth is 1 μm , the average texture depth of different cross sections texture is similar to Table 3, the load capacity of rectangular cross section is also the largest, followed by second order type ladder, circular arc, parabolic, three order type ladder and triangle. That is, the average texture depth gets closer to the initial film thickness 1 μm , the load capacity becomes greater. Figure 4b shows when the initial film thickness H_0 is 2 μm , the cross section shape has the same impact on the load capacity with Fig. 4a. That is, if the maximum texture depth H_P of different cross sections is 2 μm , the average texture depth gets closer to initial film thickness 2 μm , the load capacity becomes greater. Therefore, for the given initial film thickness H_0 and the related equal texture depth, different cross section texture can make a better choice based on the value of average texture depth and initial film thickness. The closer the average texture depth gets to initial film thickness, the greater the hydrodynamic lubrication performance of texture is.

Based on the comparison between load capacity and average texture depth with the same maximum texture depth in Fig. 4 and combining with the data of the maximum texture depth and average texture depth in Table 3, Fig. 5 shows the changing curves of maximum texture depth and average texture depth, from which we can solve the maximum texture depth H_P of different cross sections texture when the average texture depth is 1 and 2 μm . Figure 6 describes the comparison between the load capacity and maximum texture depth when the average texture

Table 3 The maximum texture depth and average texture depth of different cross sections μm

Cross section	The relation between maximum texture depth and average texture depth	0.5	1	2	4	6	8	10
Rectangular	$Y = x$	0.5	1	2	4	6	8	10
Triangle	$Y = 0.3333 * x - 0.0001$	0.167	0.333	0.667	1.333	1.999	2.667	3.333
Parabolic	$Y = 0.4626 * x + 0.0005$	0.231	0.463	0.925	1.851	2.776	3.701	4.627
Circular arc	$Y = 0.49997 * x + 0.00001$	0.25	0.499	0.999	1.999	2.999	3.999	4.999
Second order type ladder	$Y = 0.444037 * x + 0.000014$	0.312	0.625	1.25	2.499	3.75	4.999	6.25
Three order type ladder	$Y = 0.624975 * x + 0.00003$	0.222	0.444	0.888	1.776	2.664	3.552	4.44

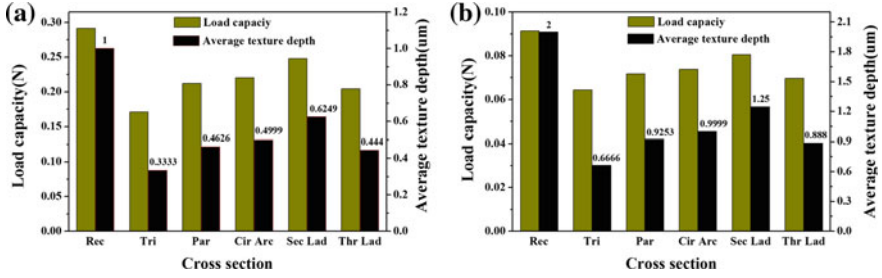


Fig. 4 Comparison between load capacity and average texture depth with the same maximum texture depth: **a** $H_0 = 1 \mu\text{m}$; **b** $H_0 = 2 \mu\text{m}$

Fig. 5 Maximum texture depth-average texture depth curve of different surface textures

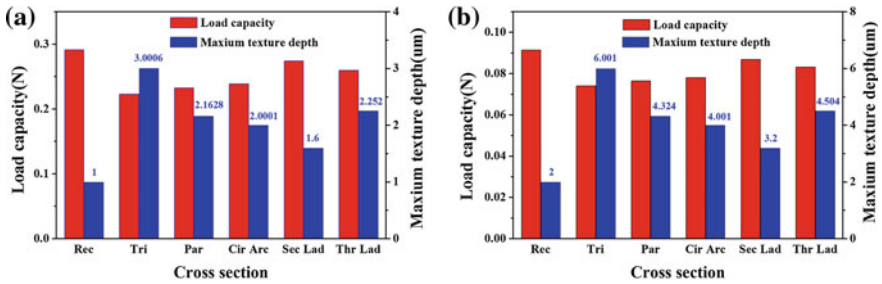
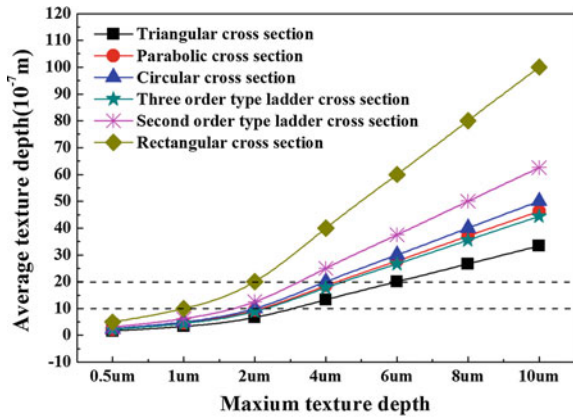


Fig. 6 Comparison of cross section-load capacity columns under the same average texture depth: **a** average depth as $1 \mu\text{m}$; **b** average depth as $2 \mu\text{m}$

depth is 1 and 2 μm , from which we can find when the average texture depth is 1 or 2 μm , the maximum texture depth of different cross sections is contrary to the average texture depth in Fig. 4 under the same maximum texture depth. However, according to Figs. 4 and 6, although the load capacity of all cross sections but rectangular is increased when the different cross sections is changed from the maximum texture depth H_p is 1 or 2 μm to the average texture depth is 1 and 2 μm , their load capacity is still smaller than that of the rectangular cross section textured surface and the relation of the load capacity of each cross section textured surface remains the same.

Figure 7a and b respectively shows the comparison of non-dimensionless film pressure when the texture of different cross sections is changed from maximum texture depth H_p is 1 μm to the average texture depth is 1 μm . According to Fig. 7, with the same maximum texture depth and average texture depth, the film pressure of different cross sections textured surface is the same as the load capacity. Namely, the greater the film pressure is, the greater the load capacity becomes. This better explains the relation of load capacity of different cross sections textured surface. However, from Fig. 7, we can find that although the load capacity of all cross sections textured surface but rectangular cross section is increased when the maximum texture depth H_p is 1 μm changed to the average texture depth is 1 μm , the relationship the film pressure of different cross sections textured surface still remains the same, which can further explain the phenomenon that the load capacity relationship of each cross section textured surface doesn't change as the load capacity is changed from Figs. 4, 5 and 6. Figure 8 shows the comparison of non-dimensionless film pressure when the maximum texture depth is 2 μm and the average texture depth is 2 μm , which has the same effect law with the film pressure of different cross section textured surface in Fig. 7.

In addition, so as to investigate the influence rules of texture cross-section shapes on hydrodynamic lubrication performance, Fig. 9 exhibits the standard deviations of texture depth as the average texture depths respectively are 1 and 2 μm . It can be

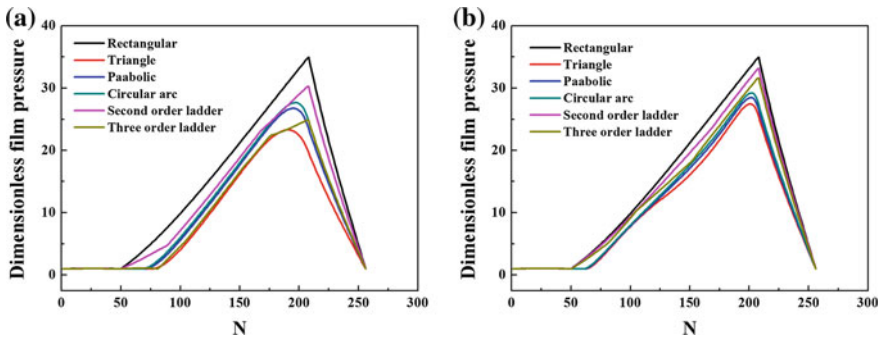


Fig. 7 Comparison of dimensionless film pressure curves with maximum texture depth and the average texture depth are 1 μm : **a** maximum texture depth as 1 μm ; **b** the average texture depth as 1 μm

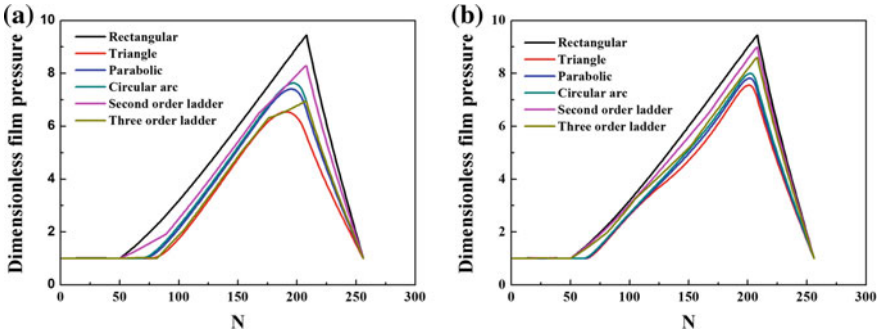


Fig. 8 Comparison of dimensionless film pressure curves with maximum texture depth and the average texture depth are $2\ \mu\text{m}$: **a** maximum texture depth as $2\ \mu\text{m}$; **b** the average texture depth as $2\ \mu\text{m}$

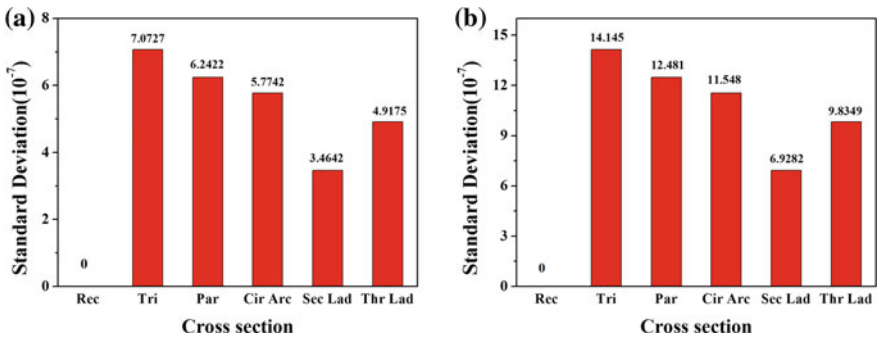


Fig. 9 Comparison of standard deviation curves with the two average depths for different shaped cross section textures: **a** the average texture depth as $1\ \mu\text{m}$; **b** the average texture depth as $2\ \mu\text{m}$

seen from Fig. 9 that the average texture depth of 1 or $2\ \mu\text{m}$ shares the same relation to standard deviations for different cross section textures, that is, the rectangular cross-section texture under these two condition both are the smallest, followed by the second order type cross section texture, the three order cross-section texture, circular-arch shaped cross-section texture, parabolic cross-section texture and triangular cross-section texture. In accordance with the definition of standard deviation, in spite of the same average depth for different shaped cross-section textures, the rates of deviation on different points in the texture differs from one another. Except for the rectangular cross section texture, textures of other cross section shape are deviated to the average texture depth at different degrees so long as they are not equal to the average depth. By the influence law of texture depth of rectangular cross section textures on the load capacity, it can be seen that the closer the texture depth is to the initial oil film thickness, the better the hydrodynamic lubrication performance would be, thus for cross section texture of

any type with the same average texture depth, the greater the corresponding standard deviation is, the greater the degree of texture depth deviates from the average depth would be and the severer texture hydrodynamic performance would be affected. Therefore, the larger the standard deviation of texture depth in different shaped cross-section textures in Fig. 9 is, the smaller the hydrodynamic lubrication effect would be and the worse the hydrodynamic lubrication performance would become. It explains that in Fig. 6, although the average depth is identical in different shaped cross-section textures, the hydrodynamic lubrication performance of different shaped cross section textured surface varies from one another.

Combined with the conclusion of selecting shapes of cross-section texture drawn based on the relationship between the average texture depth and the initial oil film thickness in Figs. 3 and 4, the optimization method of selecting shapes of cross-section texture can be further developed. In order to obtain the optimum hydrodynamic lubrication performance for any shaped cross-section texture, the smaller the standard deviation of the corresponding depth of textures and the maximum texture depth H_p , the better the hydrodynamic lubrication performance would become so long as ensuring that the average texture depth is equal to the initial oil film thickness. The mathematical expression of cross-sectional shapes is preferred:

$$\bar{h} = \sum_{i=1, j=1}^{i=n, j=m} \alpha_{ij} \min(H_p) / nm \quad (6)$$

$$f = \min \left(\sqrt{\sum_{i=1, j=1}^{i=n, j=m} (\alpha_{ij} H_p - \bar{h})^2 / (nm - 1)} \right). \quad (7)$$

where \bar{h} is the average texture depth, and i and j are respectively grid nodes along the directions of X and Y. α_{ij} is the coefficient of depths of different points on the textured surface for determining the depth values, n and m are numbers of grid nodes along the directions X and Y and H_p is the maximum texture depth.

Figure 10 depicts the comparison and contrast among surface load capacity, maximum texture depth and standard deviation of texture depth at the selected point of maximum load occurred and the average texture depth equivalent to the initial film thickness for 0.5–10 μm deep textures. It can be seen from Fig. 10a1 that when the initial oil film thickness H_0 is equal to 1 μm , the load capacity on the textured surface with two depths is almost the same, and even if the average texture depth is equal to the initial oil film thickness, the surface load capacity of the triangular cross section textured surface, the second and third order type ladder cross section textured surface are superior to that of the selected point. It also explains the rationality of making the corresponding hydrodynamic lubrication performance where the average texture depth is equal to the initial oil film thickness equivalent to the optimal texture hydrodynamic lubrication performance from Figs. 6, 7, 8 and 9. In addition to that, optimization method for texture cross section is further developed,

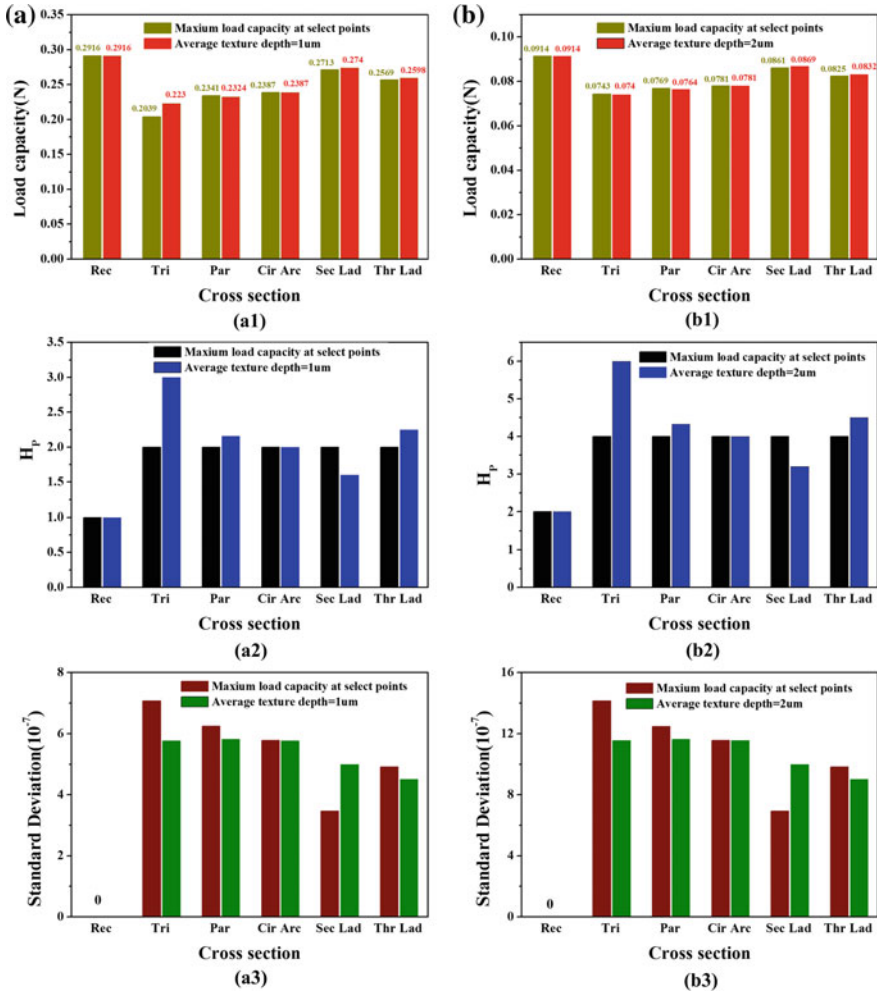


Fig. 10 Comparison of standard deviation curves of texture depth with load capacity and maximum texture depth: **a** $H_0 = 1 \mu\text{m}$; **b** $H_0 = 2 \mu\text{m}$

that is, any cross-sectional shaped texture is available to the optimal hydrodynamic lubrication performance only if the minimum standard deviation of corresponding depth of texture and texture depth H_p is ensured. However, it can be known from Fig. 10a2 and 10a3 that it not always happen that the smaller the standard deviation of corresponding depth of texture and maximum texture depth is, the greater the surface load capacity would become, thus of different cross-sectional shape textures, there is a certain difference in selecting textured cross sections shape. While for any shaped cross-section texture, the best hydrodynamic lubrication performance is gained based on the optimization method upon the average texture depth

is equal to the initial oil film thickness. Similarly, the initial oil film thickness H_0 as $2 \mu\text{m}$ in Fig. 10b has the same function rule as in Fig. 10a.

4 Conclusions

Based on the two-dimensional steady-state Reynolds equation and the texture depth equation, the theoretical model of single-structure hydrodynamic lubrication performance is proposed. The finite difference is used to discretize and solve the surface pressure distribution and then calculate the surface load capacity to analyze effect of texture shapes and depths of hydrodynamic lubrication performance and its influence law. The basic optimization method of texture cross section shapes and depths is put forward. Simulation analysis can draw the following conclusions:

1. For any shaped cross-section texture, the closer the average texture depth of different shaped cross-sectional texture is to the initial oil film thickness under the given initial oil film thickness H_0 and the same maximum texture depth H_p , the greater the surface load capacity of would be and the better the hydrodynamic lubrication performance would become. Hence, texture cross section shape can be selected based on the relationship between the average texture depth and the initial oil film thickness.
2. For any shaped cross-section texture, the textured surface can obtain better hydrodynamic lubrication performance based on ensuring the average texture depth is equal to the initial oil film thickness but not guarantee the optimal hydrodynamic lubrication performance. The optimal texture depth is selected by determining the average texture depth and the standard deviation of texture depth, but there is no uniform rule.
3. Combined with the influence law of the average texture depth on selecting the texture cross section shape and the texture depth, the smaller the standard deviation of the depths corresponding to any shaped cross-section textures and texture depth is, the better the hydrodynamic lubrication performance would become, thus the optimal texture cross-sectional shape at any texture depth can then be preferred.

Acknowledgements This project is supported by National Natural Science Foundation of China (Grant No. 51505397).

References

1. Liu YH, Wang XK, Liu PX, et al. Modification on the tribological properties of ceramics lubricated by water using fullereneol as a lubricating additive. *Sci China Technol Sci.* 2012; 1–6.
2. Fink JK. *Reactive polymers fundamentals and applications: a concise guide to industrial polymers.* Amsterdam: Elsevier Inc. All Rights Preserved; 2013.

3. Huang Z, Li Q, Zhou Y, et al. Experimental research on the surface strengthening technology of roller cone bit bearing based on the failure analysis. *Eng Fail Anal.* 2013;29:12–26.
4. Pascovici MD, Cicone T, Fillon M, et al. Analytical investigation of a partially textured parallel slider. *Proc Inst Mech Eng Part J J Eng Tribol.* 2009;223(2):151–8.
5. Marian VG, Gabriel D, Knoll G, et al. Theoretical and experimental analysis of a laser textured thrust bearing. *Tribol Lett.* 2011;44(3):335.
6. Marian VG, Kilian M, Scholz W. Theoretical and experimental analysis of a partially textured thrust bearing with square dimples. *Proc Inst Mech Eng Part J J Eng Tribol.* 2007;221(7):771–8.
7. Buscaglia GC, Ausas RF, Jai M. Optimization tools in the analysis of micro-textured lubricated devices. *Inverse Prob Sci Eng.* 2006;14(4):365–78.
8. Brajdic-Mitidieri P, Gosman AD, Ioannides E, et al. CFD analysis of a low friction pocketed pad bearing. *J Tribol.* 2005;127(4):803–12.
9. Cupillard S, Cervantes MJ, Glavatskih S. Pressure buildup mechanism in a textured inlet of a hydrodynamic contact. *J Tribol.* 2008;130(2):021701.
10. Pettersson U, Jacobson S. Textured surfaces in sliding boundary lubricated contacts—mechanisms, possibilities and limitations. *Tribol Mater Surf Interfaces.* 2007;1(4):181–9.
11. Kim B, Chae YH, Choi HS. Effects of surface texturing on the frictional behavior of cast iron surfaces. *Tribol Int.* 2014;70:128–35.
12. Shen XH, Tao GC. Tribological behaviors of two micro textured surfaces generated by vibrating milling under boundary lubricated sliding. *Int J Adv Manuf Tech.* 2015;79(9–12):1995–2002.
13. Grabon W, Koszela W, Pawlus P, et al. Improving tribological behaviour of piston ring–cylinder liner frictional pair by liner surface texturing. *Tribol Int.* 2013;61:102–8.
14. Brizmer V, Kligerman Y, Etsion I. A laser surface textured parallel thrust bearing. *Tribol Trans.* 2003;46(3):397–403.
15. Suh AY, Lee SC, Polycarpou AA. Adhesion and friction evaluation of textured slider surfaces in ultra-low flying head-disk interfaces. *Tribol Lett.* 2004;17(4):739–49.
16. Krupka I, Hartl M, Svoboda P. Effects of surface topography on lubrication film formation within elastohydrodynamic and mixed lubricated non-conformal contacts. *Proc Inst Mech Eng Part J J Eng Tribol.* 2010;224(8):713–22.
17. Tang W, Zhou Y, Zhu H, et al. The effect of surface texturing on reducing the friction and wear of steel under lubricated sliding contact. *Appl Surf Sci.* 2013;273:199–204.
18. Braun D, Greiner C, Schneider J, et al. Efficiency of laser surface texturing in the reduction of friction under mixed lubrication. *Tribol Int.* 2014;77:142–7.
19. Dobrica MB, Fillon M, Pascovici MD, et al. Optimizing surface texture for hydrodynamic lubricated contacts using a mass-conserving numerical approach. *Proc Inst Mech Eng Part J J Eng Tribol.* 2010;224(8):737–50.
20. Tala-Ighil N, Maspeyrot P, Fillon M, et al. Effects of surface texture on journal-bearing characteristics under steady-state operating conditions. *Proc Inst Mech Eng Part J J Eng Tribol.* 2007;221(6):623–33.
21. Khatri CB, Sharma SC. Influence of textured surface on the performance of non-recessed hybrid journal bearing operating with non-newtonian lubricant. *Tribol Int.* 2016;95:221–35.
22. Kango S, Sharma RK, Pandey RK. Thermal analysis of microtextured journal bearing using non-Newtonian rheology of lubricant and JFO boundary conditions. *Tribol Int.* 2014;69:19–29.
23. Sharma SC, Yadav SK. Performance analysis of a fully textured hybrid circular thrust pad bearing system operating with non-Newtonian lubricant. *Tribol Int.* 2014;77:50–64.
24. Qiu M, Delic A, Raeymaekers B. The effect of texture shape on the load-carrying capacity of gas-lubricated parallel slider bearings. *Tribol Lett.* 2012;48(3):315–27.
25. Zhang H, Hua M, Dong G, et al. A mixed lubrication model for studying tribological behaviors of surface texturing. *Tribol Int.* 2016;93:583–92.

26. Nanbu T, Ren N, Yasuda Y, et al. Micro-textures in concentrated conformal-contact lubrication: effects of texture bottom shape and surface relative motion. *Tribol Lett.* 2008;29(3):241–52.
27. Cui J, Fu Y. A numerical study on pressure drop in microchannel flow with different bionic micro-grooved surfaces. *J Bionic Eng.* 2012;9(1):99–109.
28. Ji J, Fu Y, Bi Q. Influence of geometric shapes on the hydrodynamic lubrication of a partially textured slider with micro-grooves. *J Tribol.* 2014;136(4):041702.
29. Shen C, Khonsari MM. Effect of dimple's internal structure on hydrodynamic lubrication. *Tribol Lett.* 2013;52(3):415–30.
30. Ronen A, Etsion I, Kligerman Y. Friction-reducing surface-texturing in reciprocating automotive components. *Tribol Trans.* 2001;44(3):359–66.
31. Han J, Fang L, Sun J, et al. Hydrodynamic lubrication of microdimple textured surface using three-dimensional CFD. *Tribol Trans.* 2010;53(6):860–70.
32. Papadopoulos CI, Kaiktsis L, Fillon M. Computational fluid dynamics thermohydrodynamic analysis of three-dimensional sector-pad thrust bearings with rectangular dimples. *J Tribol.* 2014;136(1):011702.

Author Biographies

Xia He born in 1976, is currently an associate professor at southwest Petroleum University, China. Research interests include the antifriction of plunger dynamic sealing tribo-pairs of fracturing pump and mechanical testing.

Wenling Liao born in 1992, is currently a master candidate at southwest Petroleum University, China. Research interests include the lubrication, friction and wear of journal bearing and downhole tools.

Guorong Wang born in 1977, is currently a professor and Ph.D. candidate supervisor at southwest Petroleum University, China. His main research interests include tribology of journal bearing and the design and simulation of downhole tools.

Mengyuan Li born in 1994, is currently a master candidate at southwest Petroleum University, China. Research interests include the lubrication, friction and wear of plunger dynamic sealing tribo-pairs of fracturing pump.